

# In situ formation of square shaped Fe<sub>2</sub>B borides in coated surface produced by GTAW

MEHMET YAZ

Vocational High School of Technical Sciences, Firat University, Elazığ, Turkey

In this investigation, a gas tungsten arc welding (GTAW) is used as a high energy density beam to form a surface over 0.15% C carbon steel with FeB and Graphite powders. The microstructure, microhardness and dry-sliding wear behavior of the composite coating were investigated using optical micrograph (OM), X-ray diffraction (XRD), scanning electron microscopy (SEM), energy dispersive X-ray analysis (EDS), microhardness tester and adhesive wear tester. A lot of types of carbide and borides were formed. Fe<sub>2</sub>B, B<sub>4</sub>C, Fe<sub>3</sub>C, FeB, Fe<sub>3</sub>B, Fe<sub>7</sub>C<sub>5</sub>, C and α-Fe phases were seen in coated surfaces. The shape of the graphite present in the FeB–C composite TIG welding coatings is various from sheet-like to spherical. Within the wear test conditions used in the present research, on Fe<sub>2</sub>B coated samples wear was essentially oxidative until the failure of the coating.

(Received August 14, 2012; accepted September 18, 2013)

*Keywords:* Fe<sub>2</sub>B, Adhesive wear, GTAW, SEM, Coating

## 1. Introduction

Different surface techniques were carried out in order to improve surfacing in situ properties of materials. Welding based surface coating methods generally include plasma transferred arc, gas tungsten arc, laser beam, submerged, electro-slag and electron beam welding procedures [1,2]. Among the weld cladding procedures, tungsten inert gas (TIG) surfacing process is a cost effective approach applied when reactive materials (as coatings or substrates) are involved [3,4].

The TIG welding process (or GTAW) is used when a good weld appearance and a high quality of the weld are required. In this process, an electric arc is formed between a tungsten electrode and the base metal. The arc region is protected by an inert gas or mixture of gases. The tungsten electrode is heated to temperatures high enough for the emission of the necessary electrons for the operation of the arc [5-8]. The solidification rate is very high during coatings by these processes. These advantages of such techniques produce rapidly solidified fine microstructures which exhibits high hardness and increased wear resistance. This technique has been used for Fe, Cr, Co, and Ni based alloy coatings synthesized on various traditional substrate materials [9].

The quality and lifetime of tools and dies are important factors in production, particularly in large batch and sophisticated production. For many years, considerable efforts have been put into attempts to increase wear resistance and service life by using different technological procedures. Attempts have been made to apply higher quality materials and adequate heat treatment, and to apply different procedures of modification and coating of surfaces in order to increase durability. Surface layers differ from the treated base material with respect to

the chemical composition, microstructure, crystal lattice, and other physical and chemical properties which result in different properties in use [10, 11].

Ferrous matrix composites have a wide range of applications because of the combination of high mechanical strength. Serious techniques are being used to produce high performance composites to improve the interfacial compatibility and avoid serious interfacial reactions. In situ technique is being used as a new technique for productions of ceramic particle reinforced metal matrix composites [12, 13].

Carburized and borided layers on AISI 1018 steel can be developed by using the GTAW technique. Increasing the carbon or boron content in the melting zone allows passing from a hypo-eutectic microstructure to a highly hypereutectic one, consisting of primary Fe<sub>2</sub>B borides and a small quantity of ferrite- Fe<sub>2</sub>B eutectic [14].

Metal Matrix Composites (MMC) with boron and carbon reinforcement exhibit significant increase in the mechanical strength and wear characteristics compared to matrix alloys and has the ability to withstand high tensile and compressive stresses by the transfer and distribution of the applied load from the usually ductile matrix to the reinforcement phase. On the other hand, these MMCs often suffer from lower ductility and inferior fracture toughness compared to the matrix and the reinforced particles are usually expensive, adding a high cost to the already aggravated final product from the costly production process. Surface modification technology comes as an alternative solution combining the superior properties of an MMC surface layer with a rather inexpensive bulk material having high ductility and fracture toughness. During the recent past, composite layers have been formed on the surface of steels using FeB and Fe<sub>2</sub>B particles in agreement with the binary Fe–B

system or CrB and Cr<sub>2</sub>B particles in agreement with the Fe–Cr–B ternary system [15].

State of the art hardfacing alloys comprise much cost efficient Fe–Cr–C or Fe–C–B systems on one hand, but on the other hand also more expensive synthetic multiphase composites reinforced with tungsten carbides for example are available. Above that, complex Fe-based alloys with niobium, titanium, molybdenum in combination with boron and carbon gained importance by achieving wear resistance due to the precipitation of different abrasion resistant hard phases and by optimized matrix properties [16–18]. Fe–C–X (X=Cr, Mn, W, Mo, Ni, B etc.) alloys are excellent candidates for hard-facing materials with surface exhibiting high wear resistance. Microstructural characterization of laser-alloyed Fe–C–X coating has demonstrated the formation of a fully martensitic phase with dislocated lath type substructures and twinned austenite needles or M<sub>7</sub>C<sub>3</sub> carbides in a dislocated ferrite matrix, depending on the concentration of Cr [19,20].

Plain carbon steels have been used industry commonly. In this investigation, the wear resistance of plain carbon steels is aimed to increase. A gas tungsten arc welding (GTAW) is used as a high energy density beam to form a surface over plain carbon steel with FeB and Graphite powders. The main objective of the present study is first of all to characterize the sliding wear behavior of the coated surfaces of the substrate with FeB and Graphite powders using a an adhesive wear apparatus and to rationalize the wear and coefficient of friction data on the basis of existing models for friction and wear.

## 2. Experimental procedure

A powdered mixture of FeB and Graphite were used as the coating material. Rectangular plates of low carbon steel (3,9370 in long, 50 mm wide and 10 mm thick) were used as substrates material. A plain carbon steel with chemical composition of 0.15% C, 0.22% Si, 0.76% Mn, 0.034% P, 0.05% S, 0.12% Cr, 0.03% Mo, 0.10% Ni, 0.52% Cu was used as the substrate material. The main chemical composition of FeB and Graphite are listed in Table 1. FeB and Graphite were mixed in four different proportions, according to Table 2. The average sizes of the ferro boron and graphite particulates were less than 50 µm. In order to obtain a homogeneous distribution of particulates, the combined powders were mixed with a blender for 1 hour. The obtained mixture has been pasted with sodium. After the process, the paste has been filled in grove opened with a grove cutter on the surface of substrate at milling machine. Samples have been dried at room temperature. The experimental conditions are also listed in Table 3. During the process, argon was allowed to flow over the processing region in order to provide a relatively inert environment. Metallographic examination of the coatings involved preparing cross sections followed by grinding from 80 to 1200 mesh and polishing with 3-µm diamond paste. For microstructural examination, the samples were etched with 100 ml HCl + 1 gr picric acid+100 ml alcohol.

The phase transformations on the coated surfaces were systematically studied by using optical (XJP-6/6A) and scanning electron microcopies combined with EDS-microanalysis and X-ray diffraction (XRD). Scanning

electron microscopy (SEM) equipped with an energy dispersive X-ray spectrometer (EDS), (JEOL JSM-7001F model of SEM, in FUENLAB). The XRD analysis was obtained by a Rigaku Geigerflex X-ray diffractometry operated at 40 kV and 30 mA using Cu-Kα radiation and X-ray diffraction (XRD). The average hard phase size and volume fraction were determined by quantitative metallography using a digital image analyzer leica Q550. Microhardness measurements were carried out using a 50 g load starting from the top to the bottom of the coatings.

Table 1. Chemical composition of reinforcements (wt%).

	Al	Si	S	Fe	B	C	P
FeB	0.07	0.44	0.025	Bal.	18.1	0.24	0.025
Graphite	-	-	-	-	-	99.9	-

Table 2. The ratio of reinforcement particulates used for coating (wt %).

Sample Number	FeB (%)	C (%)
S 1	95	5
S 2	90	10
S 3	85	15
S 4	80	20

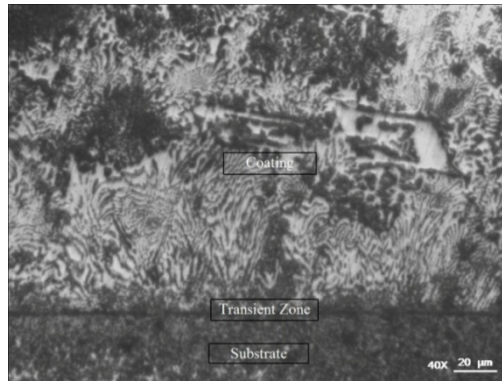
Table 3. Gas Tungsten Arc Welding parameters

Current	120 - 140 A
Speed	10 cm/min.
Shielding gas	Ar—99.9%
Shielding gas flow	14 l/min
Electrode	W–2%Th
Electrode diameter	2.4 mm

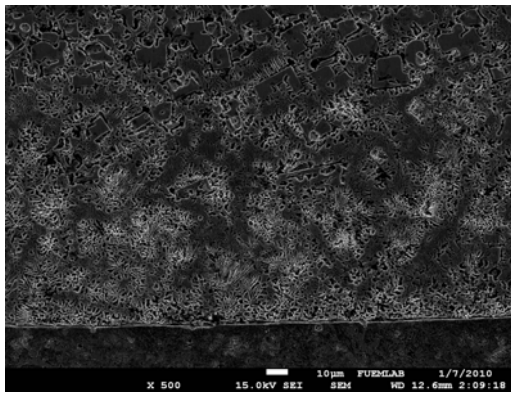
## 3. Results and discussions

### 3.1. Microstructure of coating

It was seen that the microstructure of the coated surface is not homogenous along the coating. The coated plate can be divided into three regions as seen from the microstructure of sample S1 (Fig. 1a). Transition zone SEM micrographs of sample S1 has shown in figure 1b. The transition zone (region 1) near to substrate has a hypoeutectic structure consisting of a eutectic with sorbitic pearlite islands [16, 17]. The region 2 is called as center of the coated plate, and the Fe<sub>2</sub>B borides were formed as square shape in this zone. The ratio of the square shaped Fe<sub>2</sub>B phase in region 2 is higher than the region 1. The microstructure can be phrased as squared borides in eutectic matrix (Fig. 2a). EDS analysis taken from the three different regions are given in Fig. 2b. Depending on the EDS analysis, it was postulated that the region 1 has an eutectic structure having carbides as Fe<sub>3</sub>(B,C) type (Fig 2b). Furthermore, the analyses shows that in region 2, the hard phases are Fe<sub>2</sub>B (Fig 2b), and in region 3 they are mixture of Fe<sub>2</sub>B+Fe<sub>3</sub>C borides and carbides (Fig 2b). The EDS analysis results labelled in Fig.2b is given in Table 4.

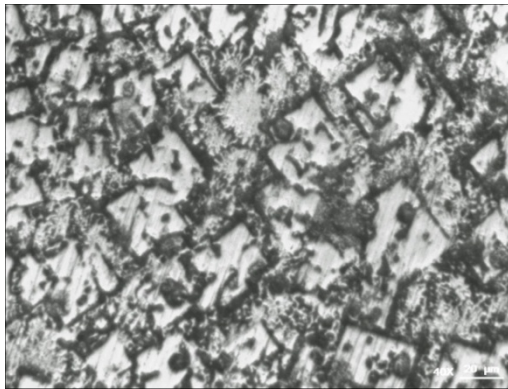


a

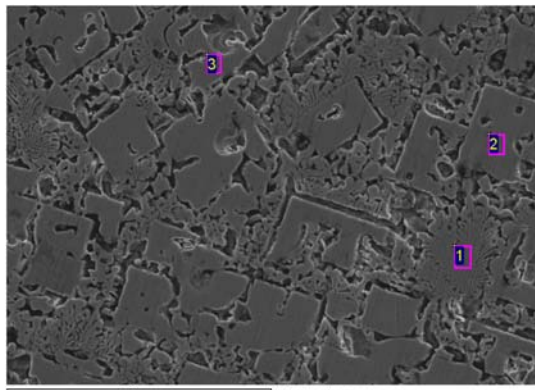


b

Fig. 1. Micrographs taken from transition zone of sample S1; a) Optical, b) SEM micrographs.



a



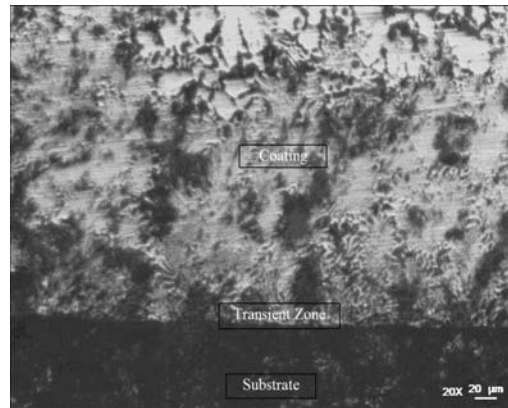
b

Fig. 2. Micrographs taken from coating center of sample S1 (Coating); a) Optical, b) SEM.

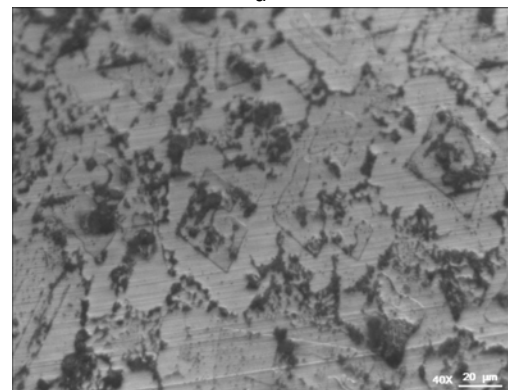
Table 4. EDS analyses of S1 taken from the microstructures labelled in Fig. 2b.

	Elements. wt %						
	B	C	Si	Mn	Fe	W	O
Point 1	7.51	7.02	0.39	0.83	83.97	--	--
Point 2	9.16	--	0.19	0.67	89.98	--	--
Point 3	8.53	7.81	0.55	0.65	77.20	1.23	4.02

The micrographs of the sample S2 were shown in Fig. 3. Similar microstructural results were seen for S2 as S1. Three different microstructural regions were seen also in the coated surface of sample S2. The eutectic structure was stiff near to transition zone, but the concentrations of square shaped boride have increased by going on the outward surface (Fig. 3a, 3b). From SEM micrographs and EDS analysis it is thought that the hard phases are Fe<sub>2</sub>B and Fe<sub>3</sub>C, and the structure of the transition zone of the sample S2 is an eutectic phase mixture (Fig.4). From the EDS analyses it can be said that boron and carbon atoms diffused toward the substrate (Table 5). The micrograph and EDS analyses taken from the second region (center of the coating) were given in Fig. 5 and Table 5, where the Fe<sub>2</sub>B borides are conglomerated.



a



b

Fig. 3. Optical micrographs of sample S2 a) Transition zone, b) Center of the coating.

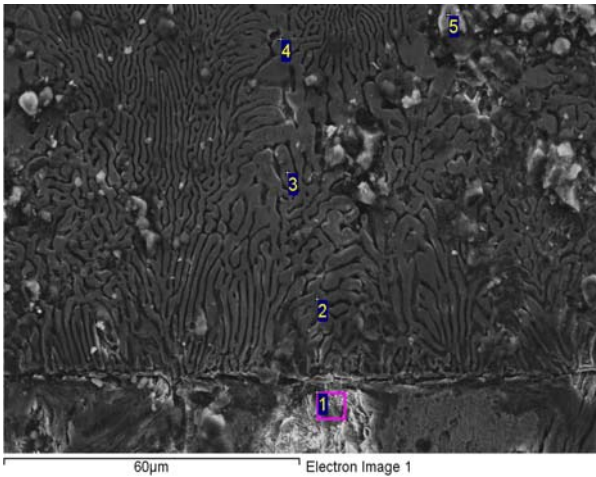


Fig. 4. SEM micrographs of sample S2; Transition zone.

Table 5. EDS analyses of S2 taken from the structure given in Fig. 4.

	Elements. wt %						
	B	C	Si	Mn	Fe	O	Cu
Point 1	6.57	13.99	0.21	0.78	64.68	10.85	2.65
Point 2	3.09	5.17	0.20	0.78	81.63	7.81	1.32
Point 3	2.12	7.63	0.21	0.81	77.43	9.85	2.25
Point 4	2.51	6.78	0.35	0.73	80.56	7.18	1.09
Point 5	8.26	25.11	1.79	0.28	30.40	32.50	--

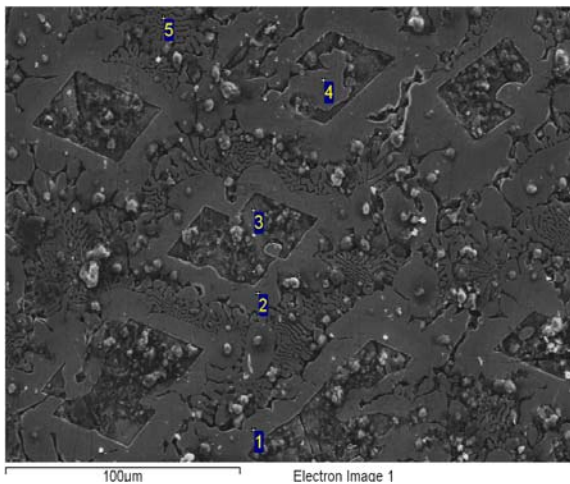


Fig. 5. SEM micrographs of sample S2; second region (center of the coating).

Table 6. EDS analyses of S2 taken from the structure given in Fig. 5.

	Elements. wt %						
	B	C	Si	Mn	Fe	O	Cu
Point 1	6.54	8.06	0.09	0.68	80.96	3.68	-
Point 2	7.73	10.30	0.11	0.58	77.09	4.20	--
Point 3	5.19	15.99	0.07	0.41	59.46	18.18	--
Point 4	6.16	9.57	0.42	0.69	73.34	9.82	--
Point 5	6.70	10.98	0.13	0.73	75.75	5.71	--

The microstructure of the Fe<sub>2</sub>B-Fe<sub>3</sub>C hard phase mixture in sample S2 was given in Fig.6. EDS analysis taken from this microstructure were labelled in Table 7.

Table 7. EDS analyses of S2 taken from the structure given in Fig. 6.

	Elements. wt %					
	B	C	Si	Mn	Fe	O
Point 1	6.25	20.18	0.17	0.21	45.79	26.69
Point 2	4.23	8.01	0.24	0.58	81.63	11.56
Point 3	6.12	5.44	0.12	0.53	84.64	7.17
Point 4	6.03	13.07	0.24	0.27	43.67	35.57

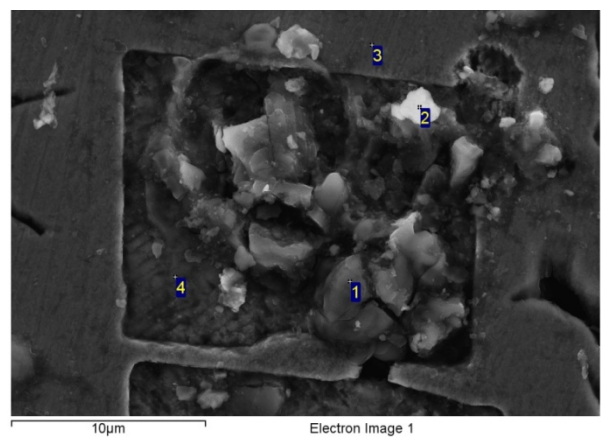


Fig. 6. SEM micrograph of sample S2; Fe<sub>2</sub>B-Fe<sub>3</sub>C.

Fig. 7a shows the microstructure of sample S3 at the interface of the borided layer and the matrix. It can be seen that liquid alloy of eutectic composition melts the matrix along the grain boundaries at high-temperature. During quickly cooling from the high-temperature, these unmelted zones are left and become islands in the eutectic [20]. On the other hand at the center of the coating it was seen that the microstructure has a large amount of eutectic structure (Fig. 7b).

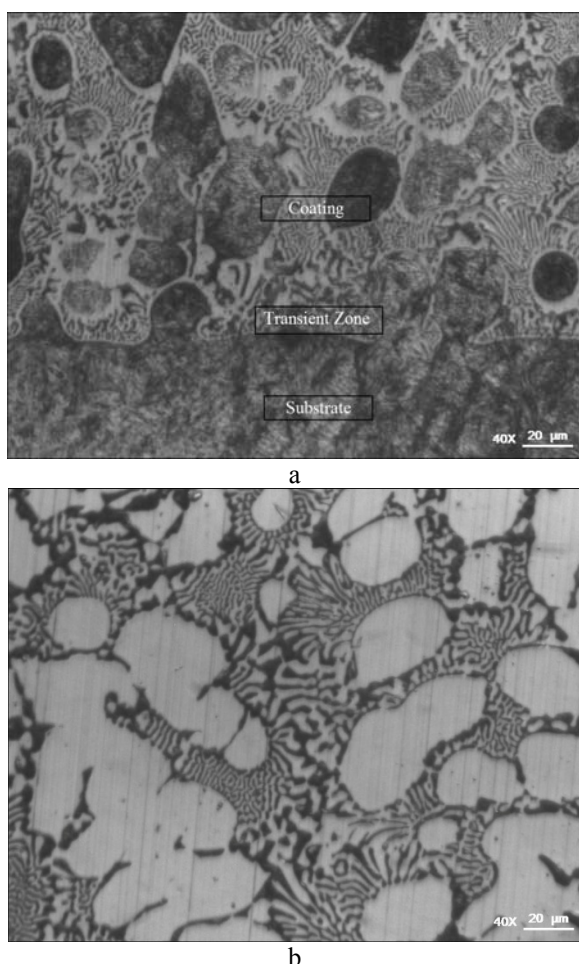


Fig. 7. Optical micrographs of sample S3 a) transition zone, b) centre of the coating

The SEM micrograph and EDS analysis taken from the center of the sample S3 supports the eutectic structure (Fig 8). In addition, EDS analysis taken from the point 1 shows that C atom diffused toward the steel side but B atoms have not diffused. The concentrations of the B atoms have increased from interface to the center of the coating. However the B atom concentration decreased again from the center to the surface of the coating. The distribution of the boron concentration has thought to be due to cooling rate of the coating (Table 8). We have seen that at the point 5, where boron concentration is minimum, the carbon concentration was at the maximum level (6.02wt. %) Carbon concentration was uniform with the exception of the area near to the surface (Table 8).

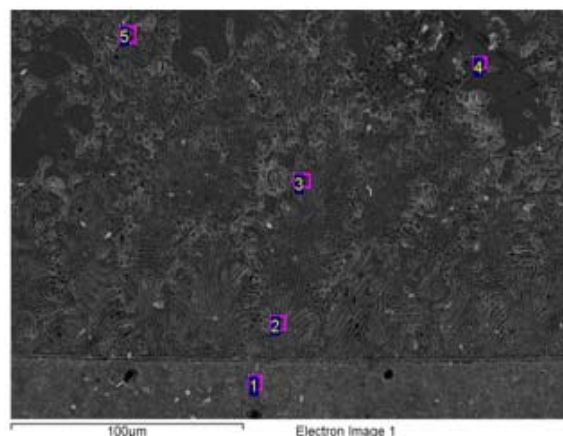


Fig. 8. SEM micrograph of sample S3; Transition zone

Table 8. EDS analyses of sample S3 taken from the structure given in Fig. 8.

	Elements. wt %					
	B	C	Si	Mn	Fe	Cu
Point 1	--	3.59	0.26	0.81	93.34	2.00
Point 2	2.91	5.69	0.04	0.60	88.95	1.38
Point 3	4.37	5.07	0.04	0.77	87.55	1.88
Point 4	4.89	4.78	--	0.57	89.42	--
Point 5	2.45	6.02	0.12	0.80	87.78	2.48

An eutectic structure formed at grain boundaries which can be seen by SEM micrograph and EDS analysis taken from the center of the coating of the sample S3 (Fig 9-Table 9). The grains are probably nonstoichiometric Fe<sub>3</sub>(B,C) phases. Moreover the C and B concentration was homogenous at grain boundaries.

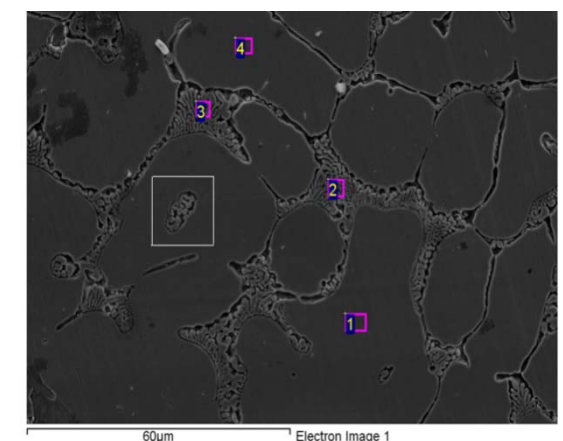


Fig. 9. SEM micrographs of sample S3 center of the coating.

Table 9. EDS analyses of sample S3 taken from the microstructure given in Fig. 9.

	Elements. wt %						
	B	C	Si	Cr	Mn	Fe	O
Point 1	2.58	3.91	0.08	0.39	0.56	92.47	--
Point 2	5.32	4.87	0.07	0.40	0.65	88.70	--
Point 3	4.79	4.50	0.03	0.29	0.87	82.68	3.39
Point 4	7.36	6.12	0.11	0.37	0.62	83.20	--

The SEM micrograph and EDS analysis of the square shape labeled in Fig. 9 were shown in Fig. 10 and Table 10. The point 1 labelled in Fig. 10 show that externally it has Si different than point 2.

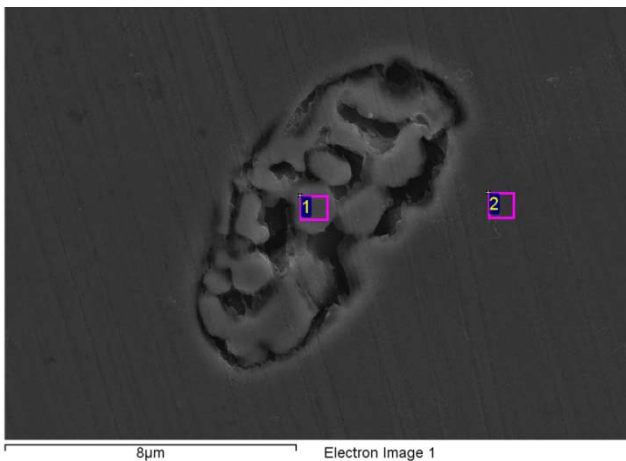
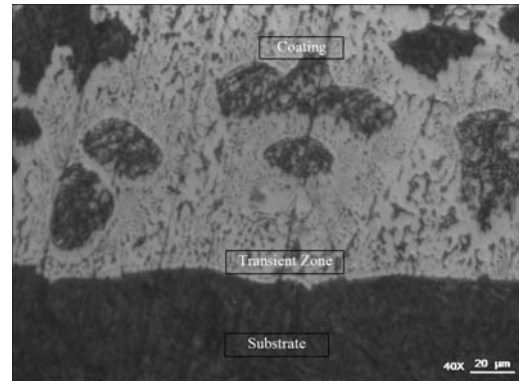


Fig. 10. SEM micrographs and EDS analyses of sample S3 (The square area that indicated in Fig. 9)

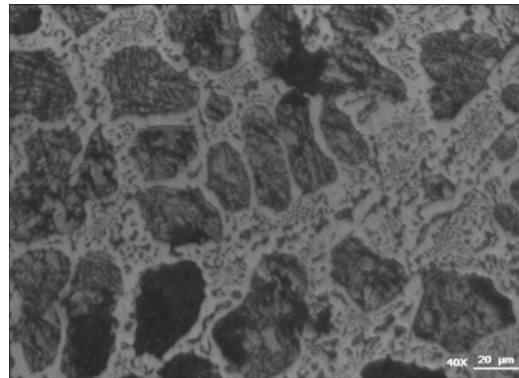
Table 10. EDS analyses results of S3 taken from the structure given in Fig. 10.

	Elements. wt %					
	B	C	Si	Cr	Mn	Fe
Point 1	6.28	4.75	0.05	0.35	0.60	87.98
Point 2	7.00	4.57	--	0.42	0.65	87.37

The coating microstructure is similar to sample S3 at transition zone and coating center of the sample S4 (Fig. 11). It can be seen that the microstructure is an eutectic structure depending on the SEM micrograph and EDS analyses given in Fig 12 and Table 11.



a



b

Fig. 11. Optical micrographs of sample S4 a) transition zone, b) center region of the coating

SEM micrograph of the sample S4 is shown in Fig. 12 where the point 1 indicates the steel side has 5.11wt.%B and 6.89wt.% C (Table 11). This result means that boron and carbon were diffused toward the steel side. Additionally, we can say that the high concentration of C-B at transition region can be understood as a good mixing before the solidification. According to other analyses taken from the transition zone (Table 11), B concentration is at the interval of 3.60-4.60wt%. On the other hand, at center of the coating (Fig. 13, point 1,2,3) the boron concentration is at 1.48-1.18wt% interval. The boron concentration was increased to 6.45wt% at the surface (Fig. 13, point 4). Similar to boron concentration, carbon concentration was also changed along cross section of coating as 5.16 to 8.42wt% (Table 12).

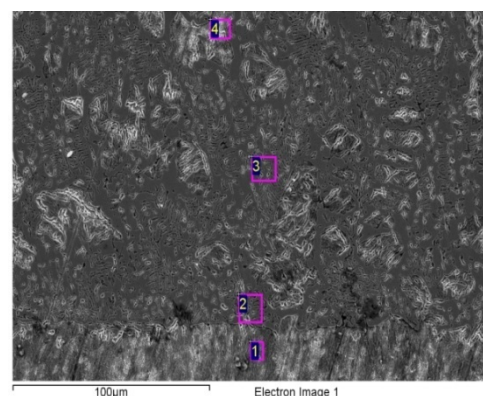


Fig. 12. SEM micrographs of sample S4; Transition zone.

Table 11. EDS analyses results of S4 taken from the structure given in Fig. 12

	Elements. wt %						
	B	C	Si	Cr	Mn	Fe	Cu
Point 1	5.11	6.89	0.43	1.10	0.84	83.18	2.12
Point 2	3.60	8.92	0.58	0.71	0.52	76.85	2.94
Point 3	4.83	6.36	0.31	1.34	0.67	85.44	1.05
Point 4	4.60	7.27	0.57	0.93	0.62	81.70	1.92

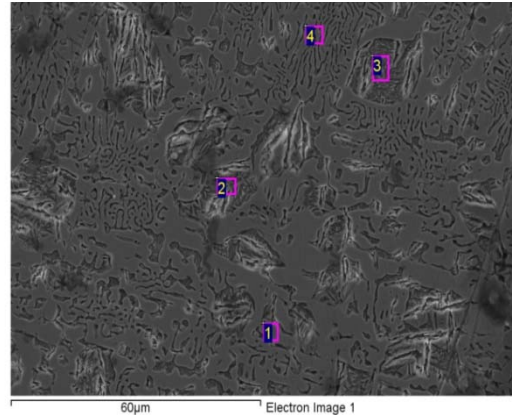


Fig. 13. SEM micrographs of sample S4 showing center of the coating.

Table 12. EDS analyses results of S4 taken from the structure given in Fig. 13.

	Elements. wt %								
	B	C	O	Si	Cr	Mn	Fe	Cu	
Point 1	2.56	8.42	4.34	0.53	1.01	0.6	80.59	1.12	
Point 2	1.38	5.16	2.80	0.83	0.61	--	86.66	2.46	
Point 3	2.23	6.41	3.02	0.74	0.71	0.59	83.76	2.54	
Point 4	6.45	7.75	--	0.26	1.25	0.54	82.64	1.12	

### 3.2. XRD Analysis

X-ray diffractions (XRD) show a lot of carbide and borides in the structure (Table 13). XRD result of the sample S1 (Fig.14) show Fe<sub>2</sub>B, B<sub>4</sub>C, Fe<sub>3</sub>C, FeB, Fe<sub>3</sub>B, Fe<sub>7</sub>C<sub>5</sub>, C and α-Fe phases at structure of the coating. On the other hand, XRD result of the sample S2 (Fig. 15) show Fe<sub>2</sub>B, B<sub>4</sub>C, Fe<sub>3</sub>C, FeB, Fe<sub>3</sub>B and Fe<sub>7</sub>C<sub>5</sub> phases.

Finally, the XRD of the sample S3 shows Fe<sub>2</sub>B, B<sub>4</sub>C, Fe<sub>3</sub>C, FeB, Fe<sub>3</sub>B, Fe<sub>7</sub>C<sub>5</sub>, C and Fe<sub>5</sub>C<sub>2</sub> phases (Fig. 17). Taking the difference between carbide and boride type into consideration, additionally Fe<sub>5</sub>C<sub>2</sub> carbide is present at the XRD result of the sample S4 (Fig. 17). The formation of Fe<sub>2</sub>B boride consumes a substantial fraction of the ductile Fe phase such that Fe<sub>2</sub>B is believed that it makes brittle the coated surface seriously [21].

Table 13. Types of carbides in the samples.

No	1	2	3	4	5	6	7	8	9	10
Carbide Type	Fe <sub>2</sub> B	B <sub>4</sub> C	Fe <sub>3</sub> C	FeB	Fe <sub>3</sub> B	Fe <sub>7</sub> C <sub>5</sub>	C	α-Fe	Fe <sub>2</sub> C	Fe <sub>5</sub> C <sub>2</sub>

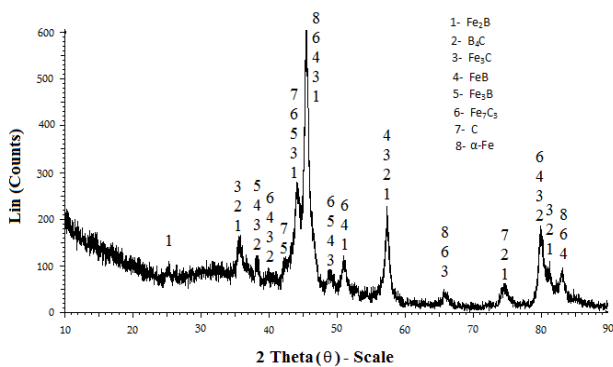


Fig. 14. XRD results of sample S1

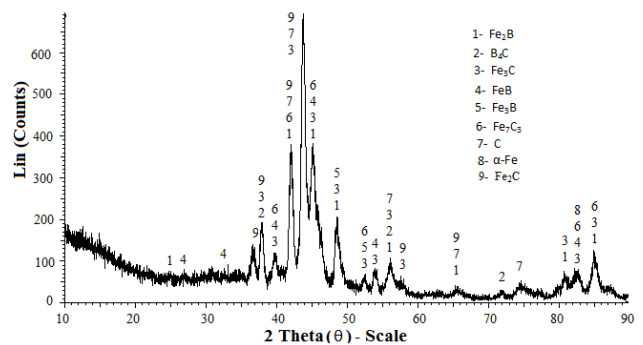


Fig. 15. XRD results of sample S2

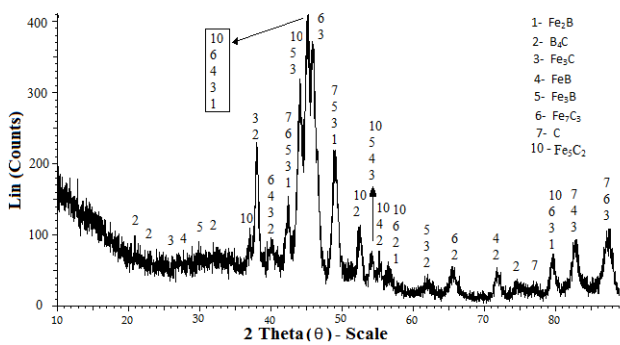


Fig. 16. XRD results of sample S3

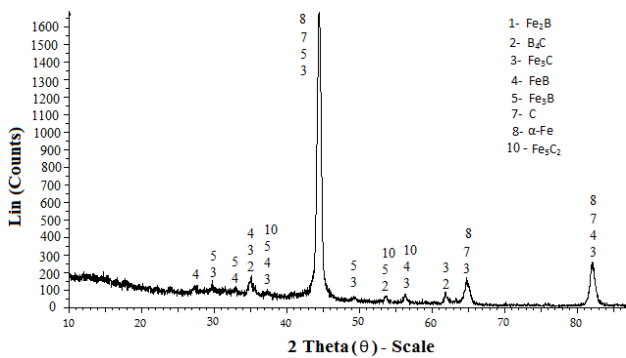


Fig. 17. XRD results of sample S4.

**3.3. Microhardness**

The microhardness results of the coating are given in Fig. 18. Sample S1 has hardness values varying between 1056 and 3450 HV. The hardness values obtained in the coating of sample S2 are changed between 1203 and 3395 HV, lower than those of sample S1. The hardness values measured in the coating of sample S3 are, between 1180 and 3277 HV. The lowest hardness measured from sample S4 are changed between 1150 and 2948 HV. As can be seen from Fig. 18, the microhardness values showed generally a slight change for all the coatings. However, a gradual decrease was seen in the transition zone. Hardness values of 814 HV, 931HV, 1180 HV and 1150 HV were measured in the transition zones for sample S1, S2, S3 and

S4 respectively. When compared with the hardness values of the coatings, this lower hardness value in the transition zone can be related to the decrease in boron content. The lower boron content in the transition zone produced softer phases as compared with the phases in the coatings. The gradual decrease of the hardness in the transition zone can be considered as advantageous because of the good adhesion of the borided layer to the substrate [14,22]. The microhardness values in the heat-affected zone of St37 steel change between 265 HV and 311 HV and decrease progressively down to 245 HV, which is the initial hardness of the substrate. In general, the results of the hardness measurement are in good agreement with the literature [14].

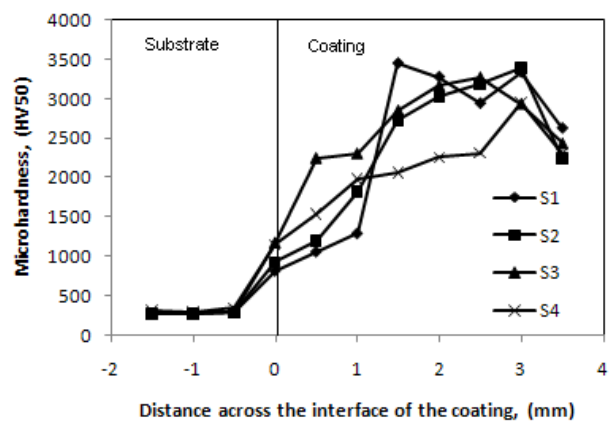


Fig. 18. The change of the micrhardness across the interface of the coating.

**3.4. Wear**

The weight loss of the sample was presented as weight loss versus sliding distance under 170 N loads by using adhesive pin-on-disc apparatus (Fig. 19). The results show that weight loss of the samples increased up to 700 M. Increasing sliding distance have show that weight loss of the samples decreased. Micrographs of the sample S3 was given in Figure 20. From EDS analysis we have seen that oxides were formed after 250 M distance.

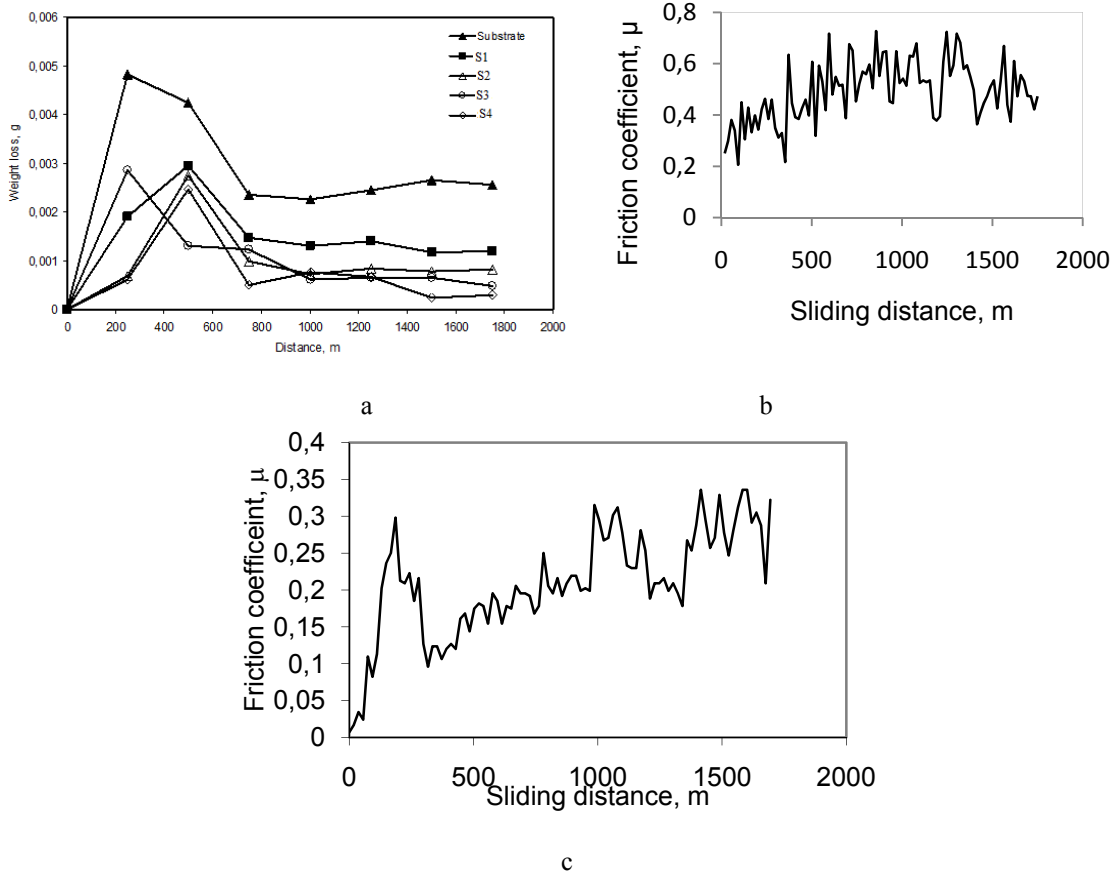


Fig. 19. a) Weight loss versus sliding distance, b) friction coefficient versus sliding distance of sample S1, c) friction coefficient versus sliding distance of sample S4.

From figure 19, it was seen that up to 258 m abrasive wear was detected for sample S3 but abrasive wear was detected up to 500 m S1, S2, S4 and substrate. Passing the 750 m, stable wear was occurred where oxides were form. From friction coefficient diagrams, it can be seen that the abrasive wear is occurred up to 300 meter for sample S1 and S4.

Table 14. EDS analyses taken from the worn surface of sample S3.(Fig. 20).

	Elements. wt %					
	B	C	O	Si	Mn	Fe
Point 1	--	9.61	5.23	0.64	0.50	83.65
Point 2	6.43	4.53	24.69	-	0.08	64.44
Point 3	7.67	2.11	37.17	-	0.07	52.60
Point 4	6.08	3.84	35.30	-	0.07	54.40

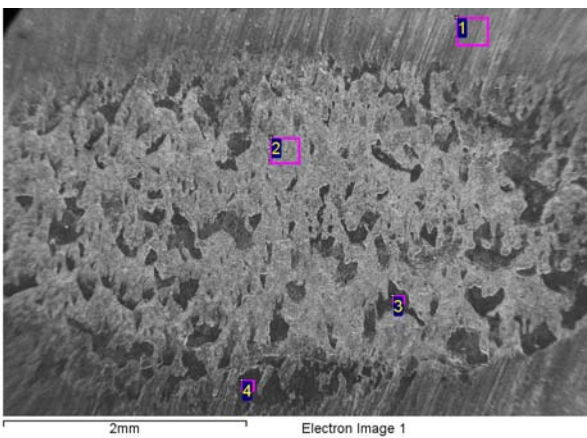


Fig. 20. SEM photograph of worn surface of sample S3.

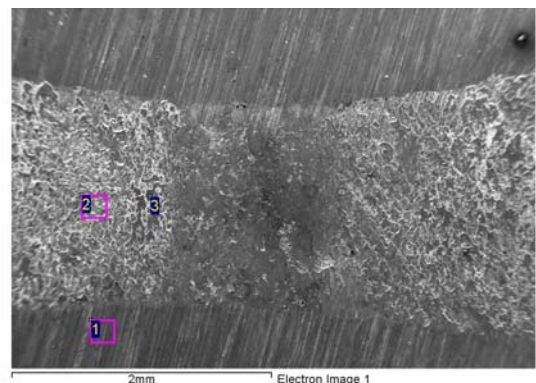


Fig. 21. SEM photograph of worn surface of sample S4.

Table 15. EDS analyses taken from the worn surface of sample S4. ( Fig. 21).

	Elements. wt %					
	B	C	O	Si	Mn	Fe
Point 1	1.66	8.15	3.64	0.48	0.56	84.36
Point 2	6.23	6.89	17.19	--	0.45	68.33
Point 3	5.34	2.83	33.83	0.04	--	55.28

From EDS analysis, it was seen that oxides of  $Fe_xO_y$  were formed on the worn surface of the samples after wear test (Table 14, Table 15.). Investigation of the table 14 and 15 show that at worn points the concentration of the Oxygen had increased.

#### 4. Conclusions

The main metallurgical reactions were occurred between FeB and C during FeB – C composite powder TIG welding processing. The metallurgical reactions between FeB and C are limited in region with a very little size at transition zone.

A lot of types of carbide and borides were formed.  $Fe_2B$ ,  $B_4C$ ,  $Fe_3C$ , FeB,  $Fe_3B$ ,  $Fe_7C_5$ , C and  $\alpha$ -Fe phases were seen in coated surfaces. B atoms in FeB particles are combined with C atoms and form various borides. The formed borides are much more stable than carbides in the composite coating. With the consolidation of the welding pool, FeB,  $Fe_2B$ , eutectics and iron-based martensite with high B contents are sequentially produced in the coatings. Some C atoms are combined with Fe together with B atoms forming the composite eutectic carbides  $Fe_3(C,B)$ . The shape of the graphite present in the FeB–C composite TIG welding coatings is various from sheet-like to spherical. The microstructure analysis shows that the shape of the graphite also depends on the FeB–C content. The distribution of the graphite in the coating is also various and depending on the powder compositions.

On the basis of the experimental results it can be concluded that the iron borides coatings, with together graphite, obtained by means of GTAW process can improve the wear resistance of carbon steel. Within the wear test conditions used in the present research, on  $Fe_2B$  coated samples wear was essentially oxidative until the failure of the coating. The weight loss of the sample S4 was the lowest, and the critical sliding distance, at which the transition from oxidative to abrasive was increased by addition of graphite from 5 to 20 wt %.

#### Acknowledgement

The author wishes to thank Firat University Scientific Research Projects Unit. This work was supported by FUBAP (Project No: 1809)

#### References

- [1] K. G. Budinski, *Welding Design & Fabrication* (1986).
- [2] W. Wu, L. Y. Hwu, D. Y. Lin, J. L. Lee, *Scripta Materialia* **42**, 1071 (2000).
- [3] K. C. Antony, J. Glenney, J. E. Northwood, *Hardfacing, Welding, Brazing and Soldering, Metals Handbook, 9th ed., Vol 6, American Society for Metals* (1983).
- [4] S. Islak, Ö. Eski, S. Buytoz, *Optoelectron. Adv. Mater. – Rapid Comm.* **6**, 665 (2011).
- [5] W. Lucas, D. Howse, *Welding and Metal Fabrication*. **64**, 1117 (1996).
- [6] P. J. Modenesi, E. R. Apolinario, I.M. Pereira, *Journal of Materials Processing Technology*, p. 260, 2000
- [7] S. Ozel, B. Kurt, I. Somunkiran, N. Orhan., *Surface & Coatings Technology*, p. 3633, 2008
- [8] C. M. Chang, C. M. Lin, C. C. Hsieh, J. H. Chen, W. Wu, *Journal of Alloys and Compounds*, p. 83, 2009
- [9] S.O. Yilmaz, *Surface and Coatings Technology*, **194**, 175 (2005).
- [10] B. Matijević, and M. Stupnišek, *Materials and Manufacturing Processes*, **24**, 887 (2009).
- [11] H. Fujita, T. Arai, *Properties and Application, Proceedings of the 4th Int. Congress of IFHT. Berlin*, p.1109, 1985
- [12] Z.Y. Ma, S.C. Tjong, L. Gen., *Scripta Materialia*, **42**(4), 367 (2000).
- [13] S.O. Yilmaz, M.Ozenbas, M.Yaz., *Tribology International*, **42**, 1220 (2009).
- [14] L. Bourithis, S. Papaefthymiou, G. D. Papadimitriou., *Applied Surface Science*, **200**(4), 203 (2002)
- [15] M. Darabara, G.D. Papadimitriou, L. Bourithis, *Surface & Coatings Technology*, **201**, 3518 (2006)
- [16] M.F. Buchely, J.C. Gutierrez, L.M. Leon, A. Toro, *Wear*, **259**, 52 (2005).
- [17] H. Berns, *Wear*, **181**, 271 (1995).
- [18] M. Kirchgaßner, E. Badisch, F. Franek, *Wear*, **265**, 772 (2008).
- [19] Xiaolei Wu, Guanguan Chen, *Material Science and Engineering*, **270**, 183 (1999).
- [20] L. Zhang, B. Liu, H. Yu, D. Sun, *Surface & Coatings Technology*, **201**, 931 (2007)
- [21] T. Teker, S. Karataş, S. O. Yilmaz, *J. Optoelectron. Adv. Mater.* **15**, 284 (2013)
- [22] M. Eroglu, *Surface & Coatings Technology*, **203**, 2229 (2009).

\*Corresponding author: myaz2623@gmail.com